Cite this: *Soft Matter*, 2011, **7**, 6313

www.rsc.org/softmatter

PAPER

Multi-functional hybrid protonated titanate nanobelts with tunable wettability†

Yuekun Lai,*[ab] Yuxin Tang,[a] Jianying Huang,[c] Hui Wang,[d] Huaqiong Li,[a] Dangguo Gong,[a] Xianbai Ji,[a] Jiaojiao Gong,[b] Changjian Lin,*[b] Lan Sun[b] and Zhong Chen*[a]

Received 9th March 2011, Accepted 3rd May 2011
DOI: 10.1039/c1sm05412k

We present the preparation of millimetre-sized liquid marbles with strong mechanical strength and good deformability using self-assembled fluoroalkylsilane functionalized titanate nanobelt powder. The strength and deformability of the marbles are adjustable by changing the intrinsic wetting state of the titanate nanoparticles. The excellent chemical stability of surface layer on the liquid marbles consisting of the titanate nanobelts provides the possibility for qualitative and quantitative chemical sensing under a wide range of pH values.

Introduction

Hydrophobic surfaces with dynamic stability are vital for a series of surface energy mediated liquid isolation applications. Liquid marble is an interesting example: since Quéré and Aussillous[1] first reported the encapsulation of water by hydrophobic particles on its surface in 2001, liquid marble has attracted increasing amount of attention due to its attractive properties that may lead to many interesting applications such as near frictionless liquid transportation, antifouling surface, reservoirs for chemical reagents, and microreactors.[2–11] The physical chemistry criteria (*e.g.* dynamic stability) of the marble depend largely on the intrinsic property of liquid core and the characteristics of shell powder being assembled at the water/air interface. Recently, great effort has been made on the investigation of pure water marbles using highly hydrophobic particles, such as fluoroalkylated lycopodium powder, silica particle or polymer latex.[12–16] However, marbles made of these materials suffer major drawbacks, including low chemical stability and low mechanical strength and flexibility. As a result, the practical applications by liquid marbles are seriously hindered. The limitations, in theory, can be overcome by searching for chemically more stable powder materials with appropriate intrinsic surface energy in order to optimize the mechanical strength of the liquid marble. In other words, stable functional powders with dynamic stability of appropriate hydrophobic property is the key to construct strong and flexible liquid marbles for practical applications. Therefore, it is of great interest to design a series of powders which enable the preparation of stable liquid marbles with controllable mechanical strength. So far the effect of powder surface hydrophobicity on the strength and deformability of its encapsulated liquid marbles has yet to be clarified.

In this work, titanate nanobelt (TNB) powders treated with different amount of fluoroalkylsilane (FAS) were shown to possess different wetting states from relatively low to very high hydrophobicity. The synthesized particles were used to prepare millimetre-sized liquid marbles which demonstrate good mechanical strength and high stretchability. It was also found that these liquid marbles exhibit excellent qualitative and quantitative gas sensing capability and long-term stability in the pH range from 0 to 14. These findings are valuable to deepen the insights into the roles of nanostructures and surface chemistry in tailoring the mechanical strength and flexibility of the liquid marbles for a series of practical applications.

Results and discussion

Fig. 1a shows the HRTEM image of the as-prepared protonated titanate nanobelts by hydrothermal method at 200 °C for 48 h followed by an acid washing process. Smooth titanate nanobelts with typically 50–200 nm in width and up to a few micrometre in length can be clearly seen. Fig. 1b provides a stabilization scheme of a TNB solution by the condensation reaction between the

[a]*School of Materials Science and Engineering, Nanyang Technological University, 50 Nanyang Avenue, Singapore, 639798, Singapore. E-mail: aszchen@ntu.edu.sg; yklai@ntu.edu.sg; Fax: +65 6790 9081; Tel: +65 6790 6727*

[b]*State Key Laboratory of Physical Chemistry of Solid Surfaces, and College of Chemistry and Chemical Engineering, Xiamen University, Xiamen, 361005, China. E-mail: cjlin@xmu.edu.cn; Fax: +86 592 2189354; Tel: +86 592 2189354*

[c]*Fujian Institute of Research on the Structure of Matter, Chinese Academy of Sciences, Fuzhou, 350002, China*

[d]*Department of Physics, National University of Singapore, 2 Science Drive 3, Singapore, 117542, Singapore*

† Electronic supplementary information (ESI) available: Video S1 shows the ultra-low adhesion to water droplet on the micro-nano structured hybrid layer on different substrates; Videos S2 and S3 show respectively the transportation of liquid marbles with low sliding resistance and strong mechanical strength; Video S4 shows the strong and flexible TNB/FAS hybrid powder film. See DOI: 10.1039/c1sm05412k

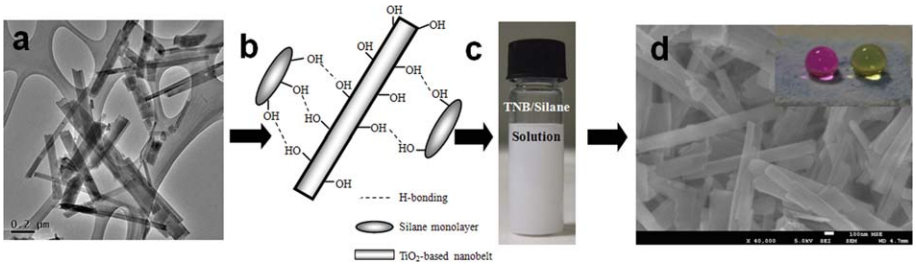

Fig. 1 (a) TEM image of the as-prepared titanate nanobelts. (b) Scheme of the stabilization of titanate nanobelts functionalized with a fluoroalkylsilane (FAS). (c) Image of the stabilized titanate nanobelt solution. (d) FESEM image of the dried TNB/FAS powder. The inset is the droplet profiles on the superhydrophobic TNB/FAS powder.

pre-hydrolysis fluoroalkylsilanol groups of FAS (–SiOH) and the surface hydroxyl groups of TNB (–TiOH). A stable TNB/FAS solution was successfully prepared by a one-step mixing of the titanate aqueous solution and a fluoroalkylsilane methanol solution under magnetic stirring (Fig. 1c). Water droplets rapidly spread and permeate into the white TNB powder indicating that the as-prepared TNB is superhydrophilic. Whereas the dyed droplets stay on the FAS grafted TNB powder surface with a ball-like shape, which indicates the readily prepared TNB/FAS surface is superhydrophobic. This unusual wetting behavior is attributed to the combination of the low surface energy of the fluoroalkyl groups and the rough structures by cross-stacked self-assembly.[17–30]

Fig. 2a presents the FTIR spectra of the as-prepared TNB powder before and after the FAS decoration. The wide absorption bank centered at 3378 cm^{-1} is due to Si–OH or Ti–OH residues. In the case of the fluoroalkylsilane modification, additional intense bands at 1212 and 1240 cm^{-1} are attributed to the stretching vibration of C–F bonds, 1124 cm^{-1} is attributed to the stretching vibration of Si–O bonds, whereas the bands at 1148 and 1066 cm^{-1} are characteristic for the formation of Si–O–C bonds.[31,32] Indeed, TEM study also revealed a shell with a thickness ~2 nm around the nanobelts thereby signaling the formation of TNB/FAS composite (Fig. 2b).[32] These results verified the successful formation of covalent bonding between the surface hydroxyl groups on nanobelts and the fluoroalkylsilanol chains.

While many techniques have been developed to fabricate superhydrophobic surfaces by creating roughened surfaces and/or changing the surface energy, these techniques are limited by the types of materials to be treated. Our approach can be simply applied to any substrate after the as-prepared highly hydrophobic TNB/FAS powder is dried as a result of the solvent evaporation. To demonstrate the versatility of the current approach, we have also prepared the superhydrophobic porous cross-stacked TNB/FAS structures on a silicon substrate, lab rubber glove and A4-size printing paper by spraying, spin coating or dip coating (Fig. 3). It is also interesting to note that the water droplet is easy to roll off due to the ultra-low solid–liquid adhesion and bounce off the glove surface when it is dropped from certain height above the surface (Video S1, ESI†).

Fig. 4 shows the stable wettability tested through water contact angles under different pH values. The average of at least three measurements taken at different positions on each sample was adopted as static contact angles. This diagram indicated that the samples remained superhydrophobic with water contact angle larger than 150° in a wide pH range from 0 to 14, which suggested the stable wettability resulted from the high chemical stability of TNB/FAS film over a wide pH range.

The as-prepared TNB/FAS hybrid powder is superhydrophobic which can float on water surface to self-assemble a tightly cross-stacked layer at the air/water interface. When a water droplet falls onto the layer of TNB/FAS hybrid powder, the water formed a spherical ball (Fig. 5a and b). Because these

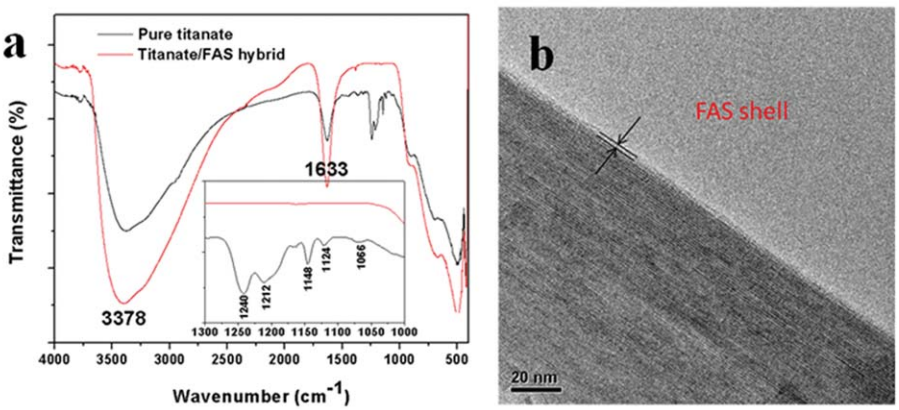

Fig. 2 (a) FTIR spectra of the as-prepared TNB powder with and without FAS modification and (b) TEM image of the TNB/FAS hybrid powder with a core–shell structure.

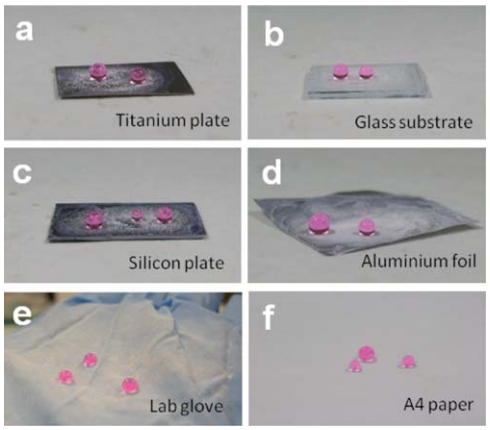

Fig. 3 Optical image of Rhodamine B (RhB) dyed water droplets of different sizes (3–15 μL) on titanium plate, glass substrate, silicon plate, aluminium foil, lab glove and A4 paper decorated with TNB/FAS hybrid powder.

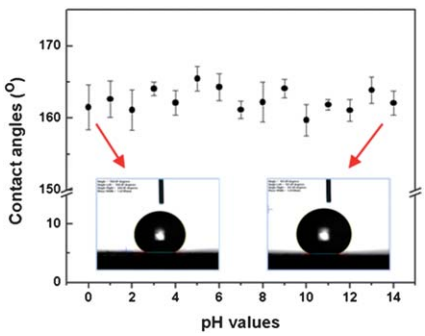

Fig. 4 Relationship between pH values and water contact angles of the TNB/FAS films on silicon plate.

cross-stacked superhydrophobic nanobelts were strongly held by the water phase (Fig. 5c), the self-assembly layer is strong enough to maintain a droplet of a few millimetres in size under impact loading. Fig. 5d–f were taken at three different focal planes of a water droplet with 1 mm in diameter. The center of the droplet

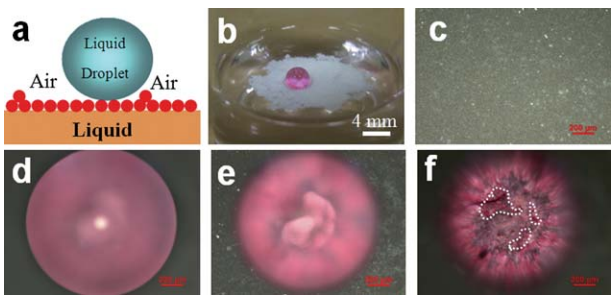

Fig. 5 Schematic representation (a) and digital image (b) of a liquid droplet sitting on the air/liquid interface covered by a layer of TNB powder. (c) Optical microscope (OM) image of the compact TNB layer self-assembled at an air/liquid interface. (d–f) OM images of a RhB colored water droplet taken at three different focal planes parallel to the equator of the droplet (d), the droplet in the vicinity of TNB surface (e), and the contact areas below the droplet (f). The red dots within three dashed graphs in (f) denote the main contact areas of the water droplet on TNB layer.

in the vicinity of TNB surface (Fig. 5e) exhibits a cloud-like shape, which corresponds to the large amount of air trapped within the liquid/solid interface.[33] The three circled areas in Fig. 5f denote the main contact areas of the water droplet on TNB layer. These contact areas matched well with the non-contact area marked by the cloud-like pattern shown in Fig. 5e.

More interestingly, the liquid marbles can be obtained by rolling a small volume of water droplet in the highly hydrophobic TNB/FAS particles (Fig. 6a). Fig. 6b shows a water marble of 1.5 mm radius dyed with Rhodamine B (RhB, 20 ppm) on A4 paper. The spontaneous encapsulation of a single layer (~30 μm in thickness) of the TNB/FAS particles around on the water droplet interface is due to the minimization of the free energy of the surface. The inset shows a contact angle of 169° between liquid marble and the substrate. Since the individual titanate particles are different in size (5–40 μm) with irregular shapes, voids exist between these particles in the self-assembled surface layer (Fig. 6c and d). The appearance of wrinkles after 60 min under 50% relative humidity was the result of water evaporation through these voids (Fig. 6e and 7a). However, water marbles are

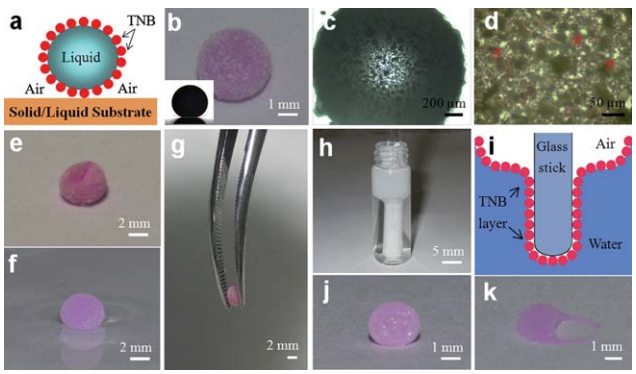

Fig. 6 Model (a) and digital image (b) of a liquid marble composed of an RhB colored water droplet coated with TNB/FAS micro/nanopowder. The inset in (b) shows the profile of a liquid marble on a solid substrate. (c and d) Top-view optical microscope images of a liquid marble. The arrows denote the voids within the TNB/FAS shell at the air/water interface. Digital image of liquid marbles on solid substrate (e) or water solution (f) after 60 min. (g) Images showing a liquid marble being picked up with a pair of tweezers. Digital image (h) and model (i) of TNB layer at the air/water interface response to intrusion by a hydrophilic glass stick. (j) Liquid marble after being released from the tweezers in a height of 2 cm. (k) Rupture of a liquid marble that was dropped from a height of 5 cm.

Fig. 7 (a) Digital photographs illustrating the effect of water evaporation on the shape of a liquid marble colored with Rhodamine B (20 ppm) after being placed on Petri dish at ambient temperature and 50% relative humidity and (b) effect of varying the solution pH on the stability of liquid marbles placed on Petri dish for 120 min.

stabilized with such TNB/FAS powder and remained floating on water for days without obvious wrinkle formation (Fig. 6f). The lifetime of a liquid marble depends on the chemical nature and porosity of the hydrophobic powder shell as well as the liquid used to form it under certain relative humidity. In Fig. 7b, we show that the liquid marbles containing different concentrations of acid or base solution with a lower surface tension can be successfully made and kept stable with slow evaporation under ambient condition by encapsulating water droplets with a shell of the TNB/FAS powder. In addition, all the water marbles colored with RhB can float and remain stable on various aqueous buffer solutions ranging from pH 0 to 13. Exception was observed at pH = 14, when the marble broke down within 8 min in the highly concentrated NaOH solution. The reduced stability is caused by the degradation of FAS in the high concentration NaOH solution. This was verified by an additional experiment where the water drop contact angle on TNB/FAS powder surface layer was observed to be unstable after some time if the powder had been soaked in pH 14 solution prior to the test. However, the powder resumed the superhydrophobic contact angle after re-applying the FAS treatment. This indicates that the FAS monolayer was degraded by the NaOH solution, not the TNB, which was formed in an even high alkalinity solution (10 M NaOH, refer to the Experimental section). The demonstrated liquid marble stability is superior to ones made by hydrophobized silica or lycopodium particles that could float, at the best, for 1 min on pure water.[34] The current work using the TNB/FAS layers has demonstrated excellent ability to encapsulate liquid with a wide range of pH values. The liquid marble can even slide without leakage on solid substrates with a small force (Video S2, ESI†), indicating the low liquid transport friction and non-contamination nature of such liquid marbles. This is attributable to the hydrophobic TNB/FAS particles self-organized on the liquid–air interface acting as an effective isolating membrane, which has trapped a great amount of air to minimize the direct contact between liquid and solid or between liquid and liquid.[24,25] In summary, the chemically inert TNB/FAS powder is insensitive to chemical reactions and resistant to acids, bases and oxidation.

Another remarkable feature of the marble by such highly hydrophobic TNB shell is its strong mechanical strength and highly deformability. For example, these marbles can be easily held by a pair of tweezers with large deformation without rupture (Fig. 6g). They can be attracted by electrostatic force and remained intact after the force is removed (Video S3, ESI†). Furthermore, a tightly packed TNB layer self-assembled on liquid surface created a highly robust and flexible superhydrophobic barrier to prevent direct contact between an inserted hydrophilic glass stick and water solution (Fig. 6h and video S4, ESI†). Water droplets larger than 3.0 mm in diameter can also stand on such tightly packed TNB layer. It was demonstrated that the robust liquid marbles could deform, rebound and finally recover to its initial spherical shape in a drop impact test from a height of 2 cm (Fig. 6j). The rupture only occurred when the drop height was 5 cm (Fig. 6k). Such a robust performance has not been achieved before, which makes these marbles a promising candidate for practical applications such as microfluidics, gas sensing, electromagnetic actuation, and microreservoirs.[1–14,34–36]

To demonstrate the effect of hydrophobicity on the strength and flexibility of the TNB/FAS membrane, different degrees of

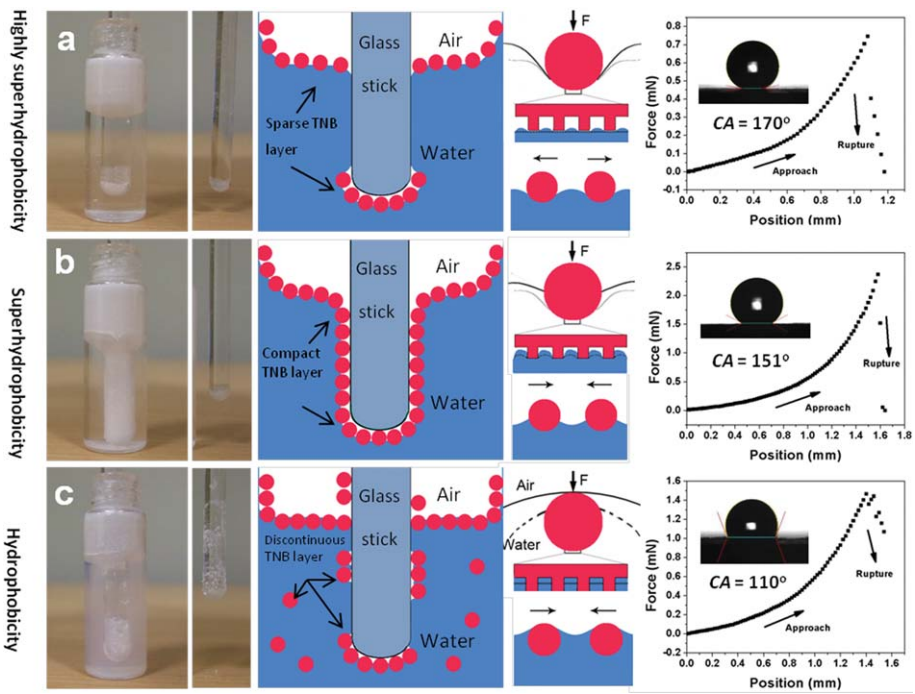

Fig. 8 The digital images and the corresponding models of the insertion of a hydrophilic rod into water covered with three types of TNB/FAS hybrid powders on the surface. The dash lines in models indicate the original state before the insertion of glass rod. The load–displacement curves show the mechanical robustness of the marbles stabilized by TNB/FAS powder with various wetting profiles (insets) under compression. (a) Highly superhydrophobic; (b) superhydrophobic; (c) hydrophobic.

wetting surface have been prepared using three types of TNB/FAS powders. They were made highly superhydrophobic (Fig. 8a), superhydrophobic (Fig. 8b), and hydrophobic (Fig. 8c) by adjusting the volume ratio of the TNB to FAS solutions to 4 : 1, 19 : 1 and 79 : 1, respectively (see details of the processing conditions in the Experimental section). The corresponding wetting contact angles are 170°, 151°, and 110° as shown in the insets. With the insertion of a glass rod, the highly superhydrophobic (CA = 170°) powder layer is easily broken. The compressive load–displacement measurement indicated that the force was only about 0.86 ± 0.21 mN (shown in Fig. 8a). This indicates that the layer has maintained the Cassie state and the water could not effectively wet through the voids between the stacked nanobelt structure even under the insertion pressure. The convex air–liquid interface induces a high repulsive force among the particles. On the other end, the hydrophobic powder with the lower contact angle of 110° was broken down by water impregnation with a comparatively higher rupture force (1.47 ± 0.25 mN, shown in Fig. 8c). We believe the insertion pressure has caused an irreversible Cassie–Wenzel transition, resulting in the breakdown of the powder layer and even powder dissolved in water. In the case of superhydrophobic TNB/FAS layer (CA = 151°, Fig. 8b), the Cassie–Wenzel transition is reversible. Under the insertion pressure, the water menisci can partially impregnate into the pores in between the particles in the surface layer, resulting in a transitional Wenzel state. Under such a state, the TNB/FAS nanobelt particles are cross-linked together and immobilized by the concave air/liquid interface and the capillary force, giving rise to the highest compression force (2.41 ± 0.32 mN) and deformation. Once the rod is retrieved from the solution, the surface recovers to its original Cassie state. With the aid of finite element analysis, we are able to deduce the elasticity modulus of the marbles. Interestingly, despite the big difference in the marble compressive break-down force, all three types of marbles display similar elasticity modulus around 0.86 KPa. This finding suggests that the elasticity of the liquid marble is largely determined by the encapsulated liquid, and the strength is affected by the surface layer tension, which is influenced by the particles and its FAS monolayer.

To verify the role of the TNB hierarchical micro/nano-structure on the marble strength, liquid marbles constructed by the commercially available Degussa P25 particles with wetting angle around 150° were found to possess a compression breaking force of 1.69 ± 0.36 mN (Fig. 9). This indicates that, in addition to the wetting angle, the cross-stacked TNB dual scale nanobelt structure plays an important role in the mechanical strength of liquid marbles.

In a qualitative NH_3 and H_2S gas sensing experiment, six groups of liquid marbles were made using distilled water, 20 ppm methyl orange solution, 0.2 M solution of $CuSO_4 \cdot 5H_2O$, $FeCl_3 \cdot 6H_2O$, $AgNO_3$ and $Cd(CH_3COO)_2 \cdot 6H_2O$ solution respectively. They were all encapsulated with a shell of the as-prepared TNB/FAS hybrid powder to form the liquid marbles (Fig. 10a). After these liquid marbles were exposed to NH_3 gas emitted from an ammonia solution (28 wt%) for 1 min, the color of the liquid marbles changes (Fig. 10b). The rapid color change of the liquid marbles is due to the porosity of the liquid marble shell, which acts as an open channel for gas transport. We can envisage that the liquid marbles with multifunctional indication or multiple marble indicators to be used to detect some specific types of gases. For examples, Fig. 10c shows the color change of the indicators in liquid marbles, which are previously exposed to NH_3 gas and then H_2S gas. In addition to qualitative vapor emission detection, the liquid marbles containing Cu^{2+} ions also show good quantitative sensing capability and correlation between the colorimetric sensing signal and the NH_3 vapor concentration (Fig. 11a). The color intensity increases with the increase of the concentration of ammonia solution. Even under ammonia solution with a low concentration of 0.875%, the color change is obvious after 5 min exposure. Therefore, the concentration of an unknown sample can be easily quantified with the color comparison, just like the pH value paper. The above results

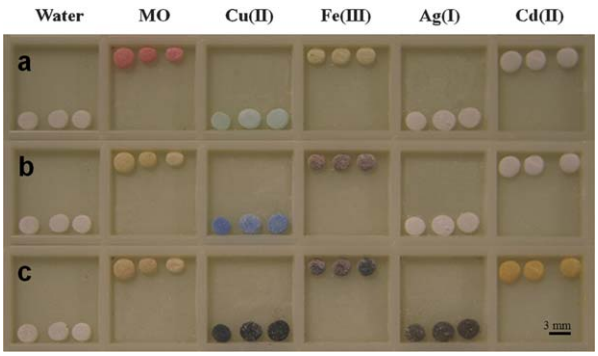

Fig. 10 (a) Six groups of liquid marbles containing de-ionized water, methyl orange, $CuSO_4$, $FeCl_3$, $AgNO_3$, and $Cd(CH_3COO)_2$ solutions, respectively, were placed from left to right. (b) The color change of these liquid marbles after exposure to ammonia gas after 1 min. (c) The color change of the marbles in (b) after further exposure to H_2S gas for 1 min.

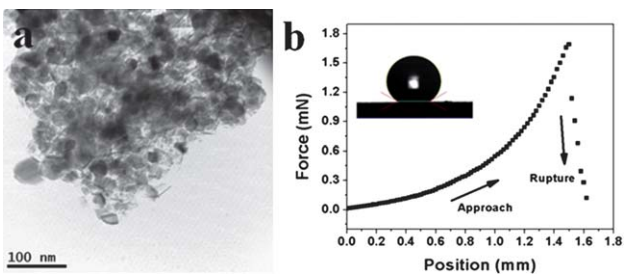

Fig. 9 (a) TEM image of P25 nanoparticles; (b) the compression force–displacement measurement of liquid marbles by P25 particles with a contact angle about 150°.

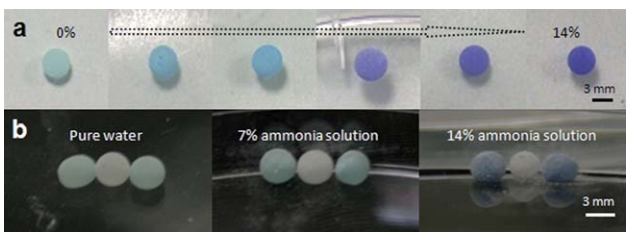

Fig. 11 Color change of the Cu(II) ion indicator containing water marble after the controlled exposure to different concentrations of ammonia solution for 1 min (a), or ammonia solution marble (center white ball) acted as NH_3 gas emitter (b) with different concentrations for 5 min.

demonstrate the potential of using such liquid marbles to perform rapid quantitative chemical analysis at a low cost and low sample volume requirement within a wide concentration range. In order to investigate the effect of marbles to be used as both a gas emitter and sensor, different ammonia solutions capsulated by the TNB/FAS powder were put in between two sensing marbles containing Cu(II) ions as the color indicator (Fig. 11b). When 7% and 14% ammonia solutions were used, the sensing marbles can effectively detect the gas emitted from nearby marble. It is also found that the marble side near the centered gas emitter has a darker color than the opposite side.

Conclusions

In conclusion, a facile one-step approach was developed to fabricate multifunctional superhydrophobic titanate nanobelt/fluoroalkylsilane (TNB/FAS) hybrid powders with controllable wettability. By optimizing the ratio of the pre-hydrolysis FAS solution to TNB powder solution, stable millimetre-sized liquid marbles with strong mechanical strength and high deformability have been successfully produced. The excellent mechanical performance is a result of the cross-stacked micro-nano dual structures with tunable hydrophobicity as we have demonstrated. Further combined with the chemical stability of the TNB/FAS hybrid powder, these marbles can be used as both qualitative and quantitative sensors capable of under diversified chemical environment.

Experimental

Preparation of titanate powders

The sodium titanate powders were prepared using a modified hydrothermal method as described in previous work.[37,38] In a typical synthesis, a 0.5 g TiO_2 (anatase) powder was uniformly dispersed in 75 mL 10 mol L^{-1} NaOH solution and then transferred into 125 mL Teflon-lined autoclave at 200 °C for 48 h. Subsequently, the as-prepared sodium titanate powder was collected and washed with distilled water, and ethanol respectively, before drying at 90 °C for 6 h. About 0.5 g of the prepared sodium titanate powder was added to 100 mL 0.1 mol L^{-1} HNO_3 solution and vigorously stirred magnetically for 15 h to produce the orthorhombic titanate ($H_2Ti_2O_5 \cdot H_2O$) through ion exchange.[39,40] Finally, the suspension was separated by centrifugation and thoroughly washed with distilled water and ethanol for five times to remove the physically adsorbed ions on the outer surface of the nanobelts completely.

Hydrophobic titanate nanobelt powder

Methanol solution of 5 g L^{-1} titanate nanobelts (TNB) and methanolic solution of pre-hydrolyzed 1 wt% 1*H*,1*H*,2*H*,2*H*-perfluorooctyltriethoxysilane ($CF_3(CF_2)_5CH_2CH_2Si(OCH_2CH_3)_3$, FAS, Degussa Co.) with a volume ratio of 4 : 1, 19 : 1, and 79 : 1 were magnetically stirred for 12 h to obtain stable opalescent solution by the creation of intermolecular interaction occurring between the nanobelts and the silanol groups. Hydrophobic TNB/FAS powder was collected and dried at 60 °C under ambient atmosphere for 60 min. Unless specifically mentioned, the results demonstrated in this paper used the powder prepared by the of TNB/FAS volume ratio of 19 : 1, which has shown the best mechanical durability.

Gas sensing

In a qualitative NH_3 and H_2S gas sensing experiment, six groups of liquid marbles were made using distilled water, 20 ppm methyl orange solution, 0.2 M solution of $CuSO_4 \cdot 5H_2O$, $FeCl_3 \cdot 6H_2O$, $AgNO_3$ and $Cd(CH_3COO)_2 \cdot 6H_2O$ solution respectively. To demonstrate the quantitative sensing capability of the liquid marbles, ammonia solutions of different concentrations (from left to right: 0%, 0.875%, 1.75%, 3.5%, 7%, and 14%) were used to act as the source of NH_3 vapor. Liquid drops of 0.2 M $CuSO_4 \cdot 5H_2O$ solution with the same volume were dropped and rolled in the TNB/FAS hybrid powder to form liquid marbles. Three identical liquid marbles were introduced into each of the above mentioned NH_3 gas vapor source. A 0.5 mL of ammonia solution with a specific concentration was dropped around the indicator-loaded marbles in the Petri dish. The Petri dish was then capped to allow the controlled exposure of the indicator-loaded marbles to ammonia solution for 5 min. At the end of the 5 min period, the Petri dish with liquid marbles was removed for taking the picture.

Characterization

Scanning electron microscopy (SEM) was performed on a JEOL JSM-7600F field-emission scanning electron microanalyzer at an accelerating voltage of 5 kV. Transmission electron microscopy (TEM) images for the TNB powder were collected on a JEOL JEM-2010 transmission electron microscope with an accelerating voltage of 200 kV. Water contact angles were measured at ambient temperature using a FTA-1000B contact angle goniometer (First Ten Angstrom, USA). The robustness of the marbles was presented through a compression test of a 10 μL marble laid in between a pair of parallel silicon plates. The test was carried out using a high sensitivity micro-electromechanical balance (Dataphysics DCAT 11, Germany) and the loading speed was 0.02 mm s^{-1}. The compressive load–displacement curve was recorded. Five tests were carried out for each experimental condition.

Acknowledgements

The authors thank the Environment and Water Industry Programme Office (EWI) under the National Research Foundation of Singapore (grant MEWR651/06/160), the National Nature Science Foundation of China (20773100, 51072170 and 20620130427), National Basic Research Program of China (973 Program) (2007CB935603), and the Technical Program of Fujian Province, China (2007H0031) for the financial support of the work. Helpful discussion with Prof. T. X. Yu (HKUST) and Dr Z. Ling (CAS) on the mechanical analysis of a compressive liquid marble is gratefully acknowledged.

References

1 P. Aussillous and D. Quéré, *Nature*, 2001, **411**, 924–927.
2 D. Quéré, *Rep. Prog. Phys.*, 2005, **68**, 2495–2532; D. Quéré, *Annu. Rev. Mater. Res.*, 2008, **38**, 71–99.
3 L. Mahadevan, *Nature*, 2001, **411**, 895–896.

4 Y. Zhao, J. Fang, H. X. Wang, X. G. Wang and T. Lin, *Adv. Mater.*, 2010, **22**, 707–710; Y. H. Xue, H. X. Wang, Y. Zhao, L. M. Dai, L. F. Feng, X. G. Wang and T. Lin, *Adv. Mater.*, 2010, **22**, 4814–4818.
5 E. Bormashenko, Y. Bormashenko, A. Musin and Z. Barkay, *ChemPhysChem*, 2009, **10**, 654–656; E. Bormashenko, Y. Bormashenko, R. Pogreb and O. Gendelman, *Langmuir*, 2011, **27**, 7–10.
6 C. S. Zhang, J. L. Xu, W. L. Ma and W. L. Zheng, *Biotechnol. Adv.*, 2006, **24**, 243–284.
7 M. Dandan and H. Y. Erbil, *Langmuir*, 2009, **25**, 8362–8367.
8 C. Dorrer and J. Ruhe, *Soft Matter*, 2009, **5**, 51–61.
9 B. W. Xin and J. C. Hao, *Chem. Soc. Rev.*, 2010, **39**, 769–782.
10 M. J. Liu, Y. M. Zheng, J. Zhai and L. Jiang, *Acc. Chem. Res.*, 2010, **43**, 368–377; L. Feng, S. H. Li, Y. S. Li, H. J. Li, L. J. Zhang, J. Zhai, Y. L. Song, B. Q. Liu, L. Jiang and D. B. Zhu, *Adv. Mater.*, 2002, **14**, 1857–1860; Y. M. Zheng, X. F. Gao and L. Jiang, *Soft Matter*, 2007, **3**, 178–182; X. Yao, Q. Chen, L. Xu, Q. Li, Y. L. Song, X. F. Gao, D. Quéré and L. Jiang, *Adv. Funct. Mater.*, 2010, **20**, 656–662; M. J. Liu and L. Jiang, *Adv. Funct. Mater.*, 2010, **20**, 3753–3764.
11 F. Shi, Z. Q. Wang and X. Zhang, *Adv. Mater.*, 2005, **17**, 1005–1009; X. Zhang, F. Shi, J. Niu, Y. G. Jiang and Z. Q. Wang, *J. Mater. Chem.*, 2008, **18**, 621–633.
12 I. A. Larmour, G. C. Saunders and S. E. J. Bell, *Angew. Chem., Int. Ed.*, 2008, **47**, 5043–5045.
13 S. H. Kim, S. Y. Lee and S. M. Yang, *Angew. Chem., Int. Ed.*, 2010, **49**, 2535–2538.
14 B. P. Binks and R. Murakami, *Nat. Mater.*, 2006, **5**, 865–869.
15 D. Dupin, S. P. Armes and S. Fujii, *J. Am. Chem. Soc.*, 2009, **131**, 5386–5387; S. Fujii, S. Kameyama, S. P. Armes, D. Dupin, M. Suzaki and Y. Nakamura, *Soft Matter*, 2010, **6**, 635–640.
16 G. McHale, D. L. Herbertson, S. J. Elliott, N. J. Shirtcliffe and M. I. Newton, *Langmuir*, 2007, **23**, 918–924; G. McHale, S. J. Elliot, M. I. Newton, D. L. Herbertson and K. Esmer, *Langmuir*, 2009, **25**, 529–533.
17 A. del Campo and E. Arzt, *Chem. Rev.*, 2008, **108**, 911–945.
18 P. Roach, N. J. Shirtcliffe and M. I. Newton, *Soft Matter*, 2008, **4**, 224–240.
19 Q. D. Xie, J. Xu, L. Feng, L. Jiang, W. H. Tang, X. D. Luo and C. C. Han, *Adv. Mater.*, 2004, **16**, 302–305.
20 M. L. Ma and R. M. Hill, *Curr. Opin. Colloid Interface Sci.*, 2006, **11**, 193–202.
21 N. J. Shirtcliffe, G. McHale and M. I. Newton, *Langmuir*, 2009, **25**, 14121–14128.
22 A. Nakajima, A. Fujishima, K. Hashimoto and T. Watanabe, *Adv. Mater.*, 1999, **11**, 1365–1368.
23 Y. C. Jung and B. Bhushan, *Langmuir*, 2009, **25**, 9208–9218; B. Bhushan and E. K. Her, *Langmuir*, 2010, **26**, 8207–8217.
24 Y. K. Lai, X. F. Gao, H. F. Zhuang, J. Y. Huang, C. J. Lin and L. Jiang, *Adv. Mater.*, 2009, **21**, 3799–3803; Y. K. Lai, C. J. Lin, J. Y. Huang, H. F. Zhuang, L. Sun and T. Nguyen, *Langmuir*, 2008, **24**, 3867–3873.
25 S. G. Park, J. H. Moon, S. K. Lee, J. Shim and S. M. Yang, *Langmuir*, 2010, **26**, 1468–1472.
26 D. A. Wang, Y. Liu, X. J. Liu, F. Zhou, W. M. Liu and Q. J. Xue, *Chem. Commun.*, 2009, (45), 7018–7020; Z. G. Guo, W. M. Liu and B. L. Su, *J. Colloid Interface Sci.*, 2011, **353**, 335–355.
27 W. Lee, B. G. Park, D. H. Kim, D. J. Ahn, Y. Park, S. H. Lee and K. B. Lee, *Langmuir*, 2010, **26**, 1412–1415.
28 M. J. Xu, N. Lu, H. B. Xu, D. P. Qi, Y. D. Wang, S. L. Shi and L. F. Chi, *Soft Matter*, 2010, **6**, 1438–1443.
29 C. R. Crick and I. P. Parkin, *Chem.–Eur. J.*, 2010, **16**, 3568–3588.
30 M. Kamperman, E. Kroner, A. del Campo, R. M. McMeeking and E. Arzt, *Adv. Eng. Mater.*, 2010, **12**, 335–348.
31 M. Peng, Z. J. Liao and Z. Zhou, *Langmuir*, 2010, **26**, 13572–13578.
32 V. Georgakilas, A. B. Bourlinos, R. Zboril and C. Trapalis, *Chem. Mater.*, 2008, **20**, 2884–2886.
33 A. B. D. Cassie and S. Baxter, *Trans. Faraday Soc.*, 1944, **40**, 546–551.
34 P. Aussillous and D. Quéré, *Proc. R. Soc. London, Ser. A*, 2006, **462**, 973–999.
35 J. F. Tian, T. Arbatan, X. Li and W. Shen, *Chem. Commun.*, 2010, **46**, 4734–4736; J. F. Tian, T. Arbatan, X. Li and W. Shen, *Chem. Eng. J.*, 2010, **165**, 347–353.
36 M. J. Sailor and J. R. Link, *Chem. Commun.*, 2005, (11), 1375–1383.
37 T. Kasuga, M. Hiramatsu, A. Hoson, T. Sekino and K. Niihara, *Langmuir*, 1998, **14**, 3160–3163.
38 Y. K. Lai, Y. C. Chen, Y. X. Tang, D. G. Gong, Z. Chen and C. J. Lin, *Electrochem. Commun.*, 2009, **11**, 2268–2271.
39 Y. X. Tang, Y. K. Lai, D. G. Gong, K. H. Goh, T. T. Lim, Z. L. Dong and Z. Chen, *Chem.–Eur. J.*, 2010, **16**, 7704–7708; Y. X. Tang, D. G. Gong, Y. K. Lai, Y. Q. Shen, Y. Y. Zhang, Y. Z. Huang, J. Tao, C. J. Lin, Z. L. Dong and Z. Chen, *J. Mater. Chem.*, 2010, **20**, 10169–10178.
40 J. J. Yang, Z. S. Jin, X. D. Wang, W. Li, J. W. Zhang, S. L. Zhang, X. Y. Guo and Z. J. Zhang, *Dalton Trans.*, 2003, (20), 3898–3901.